Article published online: 2022-09-09

Original Article

Solving the Riddle of "Idiopathic" in Idiopathic Intracranial Hypertension and Normal Pressure Hydrocephalus: An Imaging Study of the Possible Mechanisms – Monro–Kellie 3.0

Abstract

Background: Idiopathic intracranial hypertension (IIH) and normal pressure hydrocephalus (NPH) represent a cluster of typical clinical and imaging findings, with no evident etiological cause noted. In this study, we have proposed a model for IIH and NPH called Monroe–Kellie 3.0 (MK 3.0). IIH and NPH may be entities which represent opposite sides of the same coin with venous system and cerebrospinal fluid (CSF) as core drivers for both these entities. **Materials and Methods:** IIH and NPH volume data were collected, voxel-based morphometry analysis was performed without normalization, and the distribution of the individual volumes of gray matter, white matter, and CSF was statistically analyzed. Visual morphometry analyses of segmented data were performed, and the findings in routine magnetic resonance imaging (MRI) were noted to build a model for IIH and NPH. **Results:** In IIH and NPH when the volumes were compared with controls, the distribution was similar. Furthermore, the morphometric changes noted in the MRI and segmented volume data were analyzed and the results were suggestive of changes in elastic property of brain causing a remodeling of brain shape and resulting in minor brain shift in the skull vault, and the resulting passive displacement of CSF which has been termed as MK 3.0. **Conclusion:** This model helps to put the clinical and imaging findings and complications of treatment in single perspective.

Keywords: *Idiopathic intracranial hypertension, Monro–Kellie, normal pressure hydrocephalus*

Sandhya Mangalore[1,2], Srinivasa Rakshith[3], Rangashetty Srinivasa[4]

[1]Department of Neuroimaging and Interventional Radiology, NIMHANS, Departments of [2]Neuroradiology, [3]Neurosurgery and [4]Neurology, MSR INS, Bengaluru, Karnataka, India

Introduction

Idiopathic intracranial hypertension (IIH) and normal pressure hydrocephalus (NPH) are termed as idiopathic as no structural lesion is noted on imaging. A cluster of imaging features are noted which aid in making the diagnosis on magnetic resonance imaging (MRI).

IIH is a clinical condition presenting with varied signs and symptoms ranging from papilledema to headache to tinnitus to cranial nerve palsy and spontaneous rhinorrhea and spontaneous intracranial hypotension. The diagnostic imaging features range from optic nerve sheath dilatation to empty sella to prominent Meckels cave and transverse sinus (TS) stenosis.[1]

NPH, on the other hand, presents with dementia, imbalance, and urinary incontinence. The diagnostic imaging features are dilated bilateral Sylvian fissures, ventricular dilatation, and effaced high parietal sulcal spaces.[2]

The enigma of these two entities is as follows: The clinical history though suggests IIH and NPH, may not give us history on the etiology *per se*. Both these entities are chronic and progressive, with presentation extremely varied across patients.

Although there is raised intracranial pressure (ICP) in IIH, no structural lesion is visible on imaging. Imaging wise, there is impression of atrophy of frontal and parietal cortices, but there is increased pressure on digital subtraction angiography (DSA) recording in veins and high opening pressure during lumbar puncture (LP). Immediate relief of symptoms on stenting is noted as compared to cerebrospinal fluid (CSF) shunt. However, poststent, the symptoms may still recur.[3] In addition, the shunt may result in paradoxical spontaneous intracranial hypotension.[1] The core principle for all these clusters of clinical and imaging is still unknown although many theories are proposed.

In NPH, on the other hand, patients have prominent CSF spaces and increased flow

How to cite this article: Mangalore S, Rakshith S, Srinivasa R. Solving the riddle of "Idiopathic" in idiopathic intracranial hypertension and normal pressure hydrocephalus: An imaging study of the possible mechanisms – Monro–Kellie 3.0. Asian J Neurosurg 2019;14:440-52.

Address for correspondence:
Dr. Sandhya Mangalore, Associate Professor, Department of Neuroimaging and Interventional Radiology, NIMHANS, Hosur Road, Bengaluru, Karnataka, India.
E-mail: drsandym@gmail.com

Access this article online

Website: www.asianjns.org

DOI: 10.4103/ajns.AJNS_252_18

Quick Response Code:

velocity on imaging but no evident structural lesion is demonstrated and normal CSF opening pressure is noted on LP. High parietal tightness is a feature with ectatic ventricles. Although imaging features are similar to communicating hydrocephalus, the opening LP pressure is normal. The clinical presentation is over long period and only few respond to shunt.[4] Here, again, the core principle for these clusters of clinical and imaging is still unknown though many theories have been proposed.[5]

Revisiting the brain dynamics of a normal brain, we know that brain is a floating mass in the skull vault with duramater attached to the brain and skull keeping it in place, thereby avoiding shifts in the brain on movement. Hence, there is a major potential space/buffering area formed by CSF between brain and skull vault which is subdivided into multiple mini compartment/pockets, the shape and size of those are based on the duramater attached to the skull bone.

The volume of the skull vault is fixed and the pressure is maintained constant by maintaining the dynamics between the three compartments of blood parenchyma and CSF as given in the Monroe–Kellie (MK) hypothesis, that is any extra volume in one compartment leads to varying degrees of displacement in other two compartments so as to maintain constant pressure with brain, which is considered as noncompressible. Although the MK principle has proposed three compartments as core drivers, it focuses on arterial role in ICP and cerebral perfusion pressure regulation irrespective of arterial and venous CSF or brain pathology[6] [Figure 1a (i)].

MK 2.0 was proposed to focus on the role of venous pressure on intracranial veins and resulting passive increase in ICP such as venous blocks or retrograde increase in intracranial venous pressure due to increased cervical/abdominal/thoracic pressure as one of the cofactors for prognosis and outcome. The study says that subtle findings are lost if other core drivers are missed from the equation of ICP and there could be paradoxical worsening in such situations[6] [Figure 1a (ii)].

In our study, we propose MK 3.0 hypothesis, wherein we focus on the stress and strain on the brain parenchyma

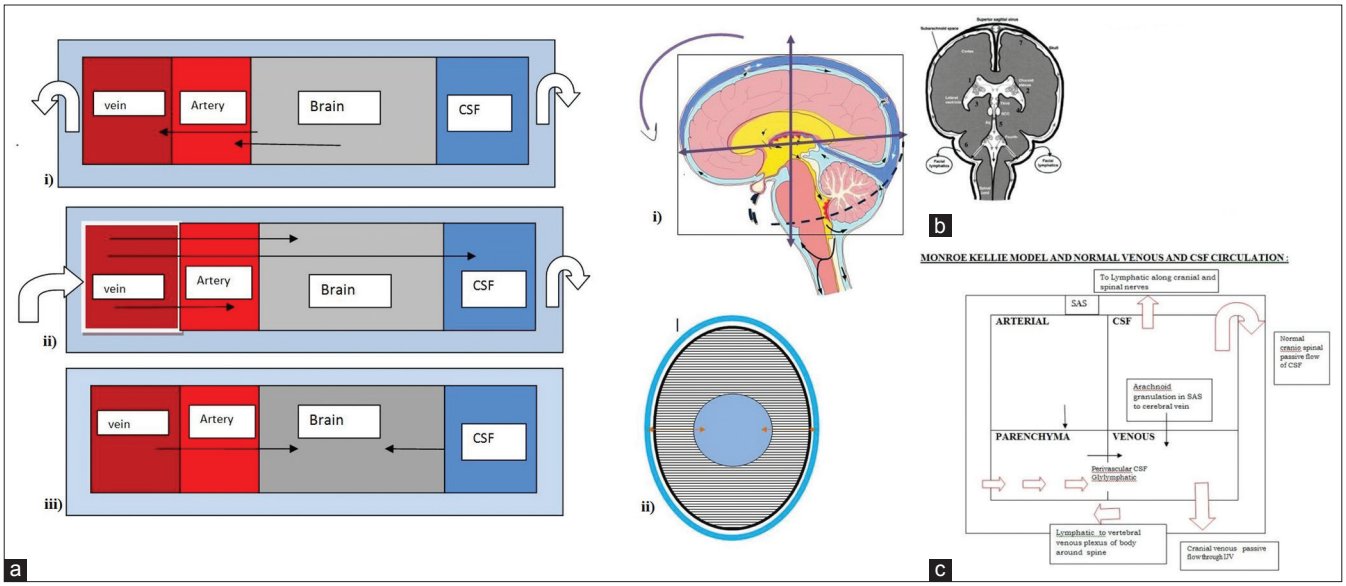

Figure 1: (a) (i-iii) Examples of Monroe–Kellie with no obvious structural lesion and three possibilities of the compensatory dynamic principles applicable. (i) Monroe–Kellie 1.0: Role of acute increase of intracranial pressure by intracranial pathology resulting in compensatory volume changes of CSF and venous volumes to maintain intracranial pressure. For example: In encephalopathy there is diffuse brain swelling and mass effect. (ii) Monroe–Kellie 2.0: Role of acute increase of intracranial pressure by intra- or extra-cranial causes of increase in venous pressure resulting in raised intracranial pressure and causing cerebral perfusion pressure arterial changes and changes in cerebrospinal fluid volumes. (iii) The now proposed Monroe–Kellie 3.0: Role of chronic process of passive increase in venous pressure in idiopathic intracranial hypertension and mirror pathology of increased cerebrospinal fluid velocity in normal pressure hydrocephalus causing shear stress and strain on the brain. There is molding in the shape and also change in the pulsatility of brain secondary to mechanical stress. (b) (i-iii) Postulated model in normal intracranial pressure with figure in sag coronal and axial. Rectangle box indicates the skull. The brain vault is broadly divided into supra- and infra-tentorial compartment and based on skull shape into anterior, middle, and posterior cranial fossa. This knowledge of compartment is important to understand cerebrospinal fluid displacement within these compartments and also to understand the skull brain interfaces. A normal brain in the skull vault has an anteroinferior tilt with subarachnoid spaces uniform around the brain parenchyma. The brain normally floats in the cerebrospinal fluid within the skull which has a fixed volume and follows a Monroe–Kelle hypothesis for equilibrium between different compartments. Normal pulsating brain reflects pulsations from the heart and as such no active pump is available in the brain, and hence the outflow of veins and cerebrospinal fluid is passive with outflow based on the displacement of extra fluid in a closed space (Monroe–Kellie model). Normal venous and cerebrospinal fluid circulation in the brain is indicated. (i) SSagittal plane image: anterior commissure is slightly inferiorly angulated as compared to posterior commissure. (ii) Axial image: The lines in the parenchyma indicate the antegrade drainage of venous blood to cerebral veins (via transmedullary veins) and the passive antegrade movement of cerebrospinal fluid (via glylymphatic system and perivascular spaces). Bidirectional arrows indicate the maintenance of equilibrium in venous and cerebrospinal fluid compartments. (iii) Coronal image: The coronal image broadly divides into supra- and infra-tentorium, with posterior fossa well above the foramen magnum and the cerebrospinal fluid flow within the craniospinal axis. (c) Monroe–Kellie model and normal venous and cerebrospinal fluid circulation

causing subtle morphological changes and resulting in minor shifts. Here, we also propose that the other two core drivers of ICP, that is veins and CSF, play a pivotal role in IIH and NPH, respectively. Further, the pathophysiology is more complicated in these two entities as no direct structural lesion is evident to match the clinical presentation and imaging findings [Figure 1a (iii)].

The hypothesis is both are passive outflow routes from brain to outside with the pathophysiology of these two being opposite side of the same coin with few similarities and few inverse relations on imaging. The imaging findings may be due to dynamic relation in which the brain is malleable to pressure and results in passive displacement of small pockets of CSF formed by dura to buffer the chronic and subtle changes induced by increased cerebral venous pressure and increased CSF velocity in IIH and NPH, respectively. In this study, though we suggest that brain is malleable along with change in shape, shear stress, and strain, it can also result in resistance with formation of a transmantle pressure gradient which differs with the pathology. Veins and CSF cisterns, on the other hand, show passive collapse or displacement upon pressure though the etiology is related to venous and CSF dynamics.

To model the MK 3.0 hypothesis, we have gathered supporting evidence from voxel-based morphometry (VBM) analysis and the cluster of morphological changes/imaging findings noted on MRI and segmented MRI data. The cause of the cluster of clinical and imaging findings may be due to these minor brain shifts in the skull vault, without any obvious pathology.

The proposed cause for brain shift in IIH is increased venous pressure in the cerebral venous sinuses. Factors such as venous variations and raised intrathoracic pressure which do not cause any structural changes on brain MRI may contribute to raised venous pressure (as noted and emphasized in MK 2.0).

The proposed cause for NPH is the increased retrograde CSF velocity which causes a strain on the brain, leading to secondary morphological changes as noted on brain MRI. The cause for increased CSF velocity could be impaired CSF absorption due to various factors in the craniospinal axis.

Our approach for this hypothesis is that we carried out a VBM analysis first to look for any volume differences as compared to controls in the segmented data, that is, gray matter (GM), white matter (WM), and CSF. Second, we have focused on the morphological changes as noted in the brain data and segmented data, and from the cluster of imaging findings unique for IIH and NPH, we have generated a model of a possible pathophysiology.

Materials and Methods

This was a retrospective-prospective study where cases of IIH and NPH were clinically evaluated and further confirmed on imaging. The imaging was done as part of clinical workup with written informed patient consent. The imaging data of the proven cases were collected for analysis. This retrospective-prospective study was approved by the Ethical Committee of MSR Medical College and Hospital as per the guidelines. The T1 volume data which are part of routine clinical MRI protocol were analyzed. The data were realigned and segmented. The segmented brain was not normalized during VBM analysis so as not to distort the brain morphology, anatomy, or skew the normal variation of volume.

The total brain volume (TBV) is a parameter which includes GM, WM, and CSF volumes, whereas intracranial volume measures the total of GM and WM.

Retrospective and prospective data collection was done for 15 cases of IIH and NPH. The MPRAGE data were collected after a clinical and radiological diagnosis of IIH or NPH was done. T1 volume data were collected and processed for supporting the hypothesis. Individual MRI images of patients were also studied for the second part.

Results

Volume of GM, CSF, and WM is almost similar with no significant difference in the volumes of GM, WM, and CSF as noted in the scatter plot. The TBV and the intracranial volume were also similar in both the cases [Figure 2a (i-v)].

Morphological differences in shape were noted visually and will be discussed. Figure 2b (i-iv) represents GM, WM, and CSF segmented data in a control, IIH, and NPH case, respectively. On GM template, we looked for any shape changes, whereas on WM segment, we looked for corpus callosum (CC) and brainstem morphology. On CSF segment, we looked for morphology changes in the cisterns and ventricle. We observed that the CSF segment gave us a good knowledge of the CSF cisterns and the shape morphology was better seen on this segment as it gives a ventriculogram-like picture and shape of the brain in this silhouette was better appreciated.

Regular MRI images were looked for to assess for extracranial CSF pathways such as optic nerve, Meckels cave, and spinal nerve roots. If additional imaging such as magnetic resonance angiography and magnetic resonance venography were available, their findings were noted [Figures 3 and 4].

Furthermore, broadly, the intracranial structures are compartmentalized by tentorium as supratentorium (anterior cranial fossa [ACF] and middle cranial fossa [MCF] structures, central brain, and parietal convexity) and infratentorium.

The morphological changes in the supratentorial and infratentorial compartments on segmented brain and regular MRI have been described and summarized below

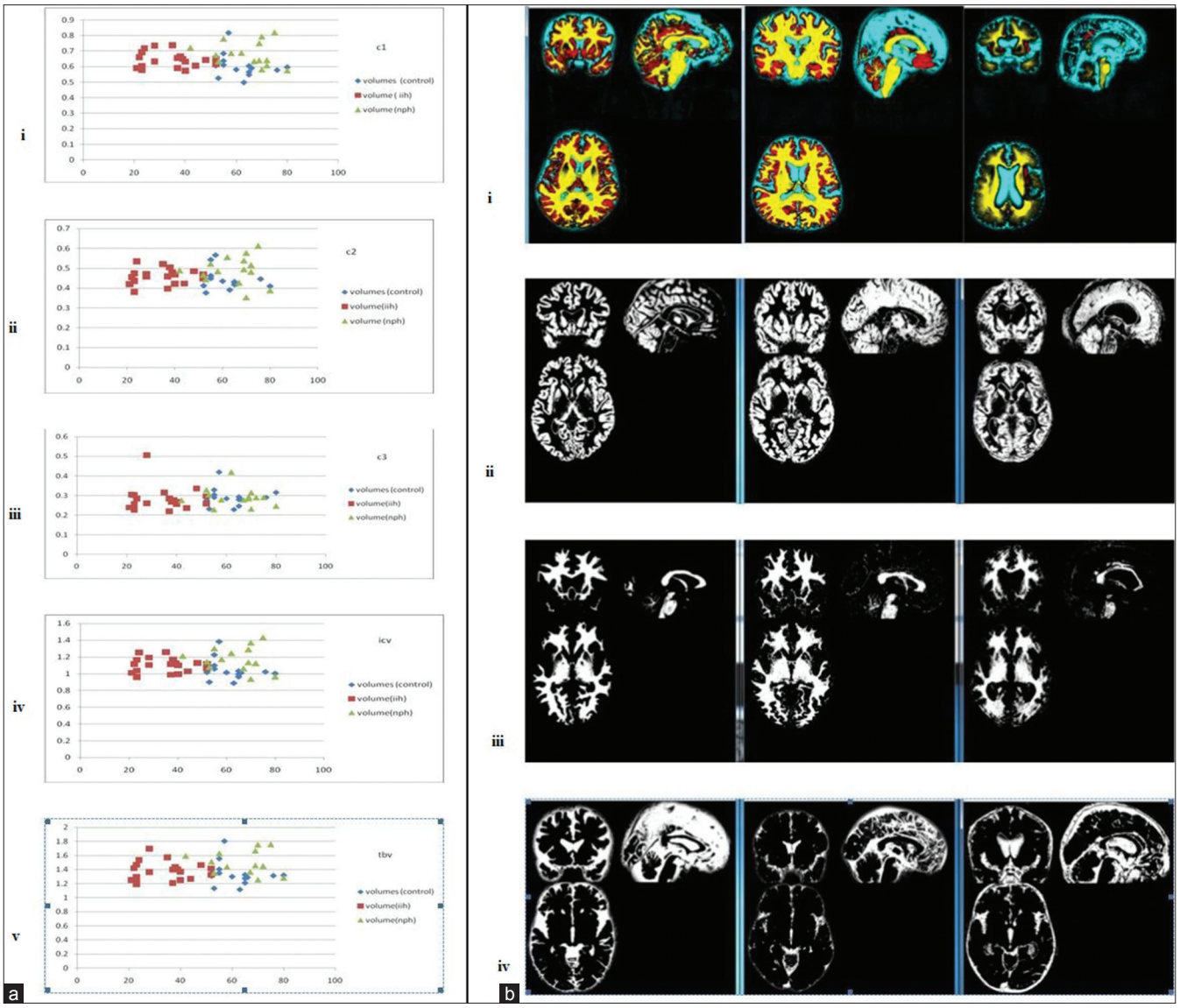

Figure 2: (a) (i-v) The scatter plot of the gray matter, white matter, and cerebrospinal fluid volumes along with intracerebral volume and total brain volume. X-axis represents the age and Y-axis represents the volumes. The volume after voxel-based morphometry analyses of T1 data is similar in all the three groups with an incidence of idiopathic intracranial hypertension more in the younger age group (C1: Gray matter volume, C2: white matter volume, C3: cerebrospinal fluid volume, C1+C2: intracerebral volume, C1+C2+C3: total brain volume). (b) (i) Morphological evaluation of the segmented data in the control, idiopathic intracranial hypertension, and normal pressure hydrocephalus cases. Fused gray matter, white matter, and cerebrospinal fluid segmented images of single patient. Yellow: white matter, red: gray matter, and blue: cerebrospinal fluid. No normalization of shape or intensity was carried out. (ii-iv) Segmented (ii) gray matter, (iii) white matter, and (iv) cerebrospinal fluid data to look for any morphological changes in normal controls, idiopathic intracranial hypertension cases, and normal pressure hydrocephalus cases

in Table 1. Overall, the results in IIH and NPH looked like venous and CSF pathology contributing to the pathology.

Because it is a chronic pathology, there were features of gradual shift of the central/medial brain structures in a downward direction in IIH (increased venous pressure and volume) and upward direction in NPH (increased CSF velocity). In the lateral aspect, the CSF was passively displaced within compartments, the margins of which were formed by dura or bone. In supratentorium, CSF was displaced between ACF, MCF, and parietal convexity structures.

In infratentorium, there was a shift of central/medial brain structures (brainstem) in downward direction/buckling in IIH and upward shift/straightening of brainstem. In addition, for the midline vermis and cerebellum, there was counterclockwise rotation when pushed inferiorly (up to down) in a case of IIH and clockwise rotation when pushed down to up in a case of NPH.

Discussion

Typically, ICP of brain is based on MK which focuses on arterial role as core driver, whereas recent hypothesis (MK 2.0) focuses on vein as the core driver of maintaining ICP. Lack of

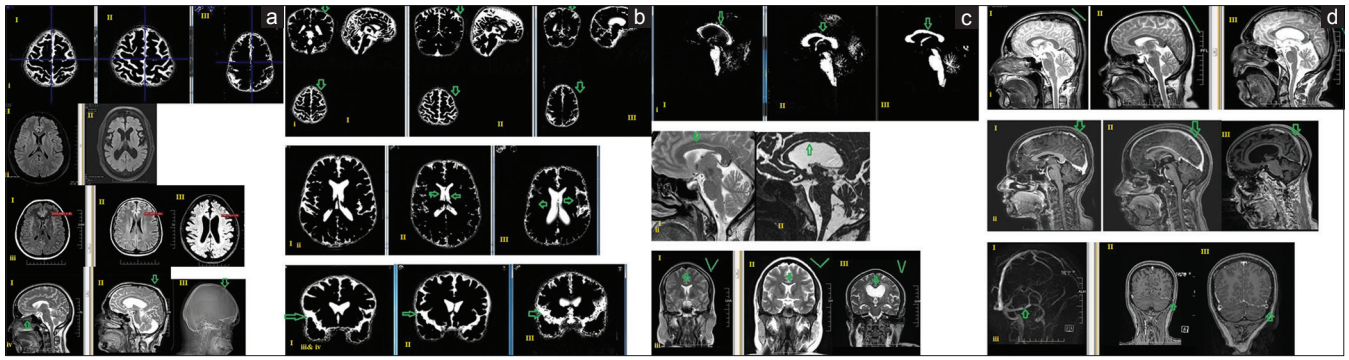

Figure 3: (a) (i-iv) Whole-brain analysis findings in normal controls, idiopathic intracranial hypertension cases, and normal pressure hydrocephalus cases. (i) cerebrospinal fluid segment giving a ventriculogram-like image: (I) normal shape of the brain, (II) idiopathic intracranial hypertension of the brain has a brachy appearance, (III) normal pressure hydrocephalus of the brain has a dolicho appearance in high-convexity cuts, (ii) Gray–white differentiation: (I) Idiopathic intracranial hypertension: gray–white differentiation increased due to venous congestion and white matter > gray matter appears hypointense, (II) normal pressure hydrocephalus: gray–white differentiation maintained, (iii) Pixel value at window level 131 and window width 156: (I) Idiopathic intracranial hypertension: gray–white differentiation, increased white matter appears hypointense with value 81, (II) normal gray–white differentiation: fluid-attenuated inversion recovery images: window level 131 and window width 156 with pixel value 131, (III) normal pressure hydrocephalus: gray–white differentiation maintained, but white matter appears more hyperintense with a value of 170, (iv) Polar opposite findings: (I) idiopathic intracranial hypertension thinned out ethmoid bone and remodeling of sella, (II/III) normal pressure hydrocephalus silver beaten- appearance of parietal bone on MRI and CT. (b) (i-iv) Cerebrospinal fluid segment at high convexity: (i) (I) normal, (II) idiopathic intracranial hypertension parietal convexity > high frontal subarachnoid space is prominent, (III) normal pressure hydrocephalus parietal convexity >> high frontal subarachnoid space is effaced (hallmark sign). (ii) cerebrospinal fluid segment at lateral ventricle level: Ratio of lateral ventricle and subarachnoid space: (I) normal ratio of lateral ventricle and subarachnoid space, (II) idiopathic intracranial hypertension: decreased size of both lateral ventricle and subarachnoid space, (III) normal pressure hydrocephalus: increased size of both lateral ventricle and subarachnoid space. Line of torque and subarachnoid space: (I) normal frontal and occipital subarachnoid space, (II) idiopathic intracranial hypertension: decreased size of prefrontal and occipital subarachnoid space, (III) normal pressure hydrocephalus: decreased size of prefrontal and occipital subarachnoid space (line of maximum torque at the ventricle level [refer model]). (iii) Cerebrospinal fluid segment: midcoronal view Sylvian fissure: (I) normal Sylvian fissure, (II) idiopathic intracranial hypertension slightly effaced out, (III) normal pressure hydrocephalus: prominent Sylvian fissure (hallmark sign). (iv) The temporal lobe configuration against the base of anterior cranial fossa in coronal plane is assessed: (I) normal temporal lobe with cerebrospinal fluid, (II) idiopathic intracranial hypertension: the subarachnoid space appears effaced with temporal lobe appearing mildly large in coronal plane, (III) normal pressure hydrocephalus: subarachnoid space and Sylvian fissure prominent with temporal lobe appearing flattened in the coronal plane. (c) (i-iii) White-matter segmented image showing the anatomy of (mid sagittal image) central structures: corpus callosum, brainstem, and cerebellar white matter. (i) Corpus callosum: the images are flipped horizontally (I-III) (I) normal pressure hydrocephalus, (II) idiopathic intracranial hypertension, (III) normal. (I) Normal pressure hydrocephalus: thinned out corpus callosum due to stretching of corpus callosum and the anterior commissure higher than posterior commissure, (II) idiopathic intracranial hypertension: increased thickness/density due to foreshortening of corpus callosum and posterior commissures appear inferior to anterior commissures. (III) Normal configuration and thickness of corpus callosum and the anterior and posterior commissure relation. (ii) The corpus callosum shape: (I) idiopathic intracranial hypertension: waviness of the outer surface of corpus callosum and is directed downward, (II) normal pressure hydrocephalus: waviness of the inner surface of corpus callosum and is directed upward. (iii) Callosal angle coronal: (I) normal, (II) idiopathic intracranial hypertension maintained but have an elongated profile, (III) normal pressure hydrocephalus ballooned out and reduced angle. (d) (i-iii) Tentorium and venous sinus (i and ii) T2 sagittal and (ii) post contrast: (I) Normal tentorium length position along the venous sinus (shown as a green line parallel to straight sinus, (II) idiopathic intracranial hypertension: tentorium stretched with a downward angulation and appears to have prominent venous sinus, (III) normal pressure hydrocephalus tentorium stretched and appears to have downward angulation with normal sinus diameter (iii) in a case of idiopathic intracranial hypertension, (I) magnetic resonance venography (II and III) postcontrast image showing a large arachnoid granulation in the transverse sinus

pulsation perioperatively due to change in the elastic property of brain is noted. The entity of active resistance offered by brain parenchyma to pressure and passive displacement of CSF in various location in response to increased ICP has not been explored for which we have termed MK 3.0. Computational deformation models show transmantle pressure gradients in IIH and NPH,[7] Virchow–Robin (VR) spaces, and glymphatic drainage.[8,9] Other unconventional routes of CSF drainage such as perineural spaces are also being studied in IIH and NPH.[10,11]

IIH and NPH are chronic disorders and based on stretching of the veins have a specific distribution pain pattern.[6] IIH appears more malignant than NPH clinically. NPH appears benign with gait abnormality dementia.[1,2]

Unlike active pulsatile inflow of arteries, venous and CSF flow are passive outflow routes. Sudden decrease in outflow of venous return (cerebral venous thrombosis [CVT]) or CSF outflow (obstructive hydrocephalus) can cause increase in ICP, with MRI features of coning of brain. In IIH and NPH, there is chronic, subtle, and progressive increase of venous pressure and decreased CSF absorption, respectively, leading to decreased outflow and with secondary compensatory phenomenon occurring such as molding of shape of brain parenchyma, shift of CSF in subarachnoid space (SAS) from one compartment to another (within the individual cranial fossa), and at CSF drainage sites. A differing transmural gradient of resistance is offered to the increased pressure or velocity across the brain parenchyma.

A model of the vicious cycle for pressure buildup in IIH and NPH and the relevant imaging findings has been built in this study. A study on glylymphatics in IIH has shown that, similar to NPH, there was impaired drainage of gadolinium, secondary to impaired glylymphatic clearance.[12] Enlarged foramen ovale and jugular foramen are noted due to remodeling as seen in IIH, which are also routes of CSF drainage along nerve sheath. IIH is noted as raised

Table 1: Results of imaging findings

Summary of the morphological changes in the brain in IIH and NPH		
Controls	**IIH**	**NPH**
	Whole brain	
Volume of gray-white CSF	Similar distribution as controls of gray–white CSF and TBV and ICV	Similar distribution as controls of gray–white CSF and TBV and ICV
Shape of brain parenchyma	Brachy appearance	Dolicho appearance
Venous congestion	The white matter appears more hypo and gray white distinction increased on a FLAIR image	The FLAIR image appears normal to hyperintense
Skull bone	Thinned-out ethmoid bone (CSF leak is known clinically)	Silver beaten appearance of the inner wall of the skull (parietal convexity)
	Widened and enlarged sella due to bone remodeling	
Supratentorial structures (ACF and MCF): Frontal parietal occipital and temporal lobes		
High frontal and high parietal structures (convexity level)	High parietal >> high frontal SAS prominent	High parietal >> high frontal SAS effaced
Frontal and occipital SAS (lateral ventricle level) line of torque	Decreased size of SAS in prefrontal and occipital poles	Decreased size of SAS prefrontal and occipital poles
		Prominent parieto-occipital fissure
Ratio of lateral ventricle and SAS (lateral ventricle level) (axial and coronal views)	Decreased size of both lateral ventricle and SAS	Increased size of both lateral ventricle and SAS
Temporal lobe at the level of temporal horn of lateral ventricle	The SAS appears effaced, with TL appearing mildly prominent in the coronal plane (deformation of shape)	The SAS and Sylvian fissure prominent, with TL appearing flattened in the coronal plane (deformation of shape)
Midline structures in sagittal and coronal planes: CC, tentorium, and veins		
Corpus callosum shape and thickness (deformity assessment)	Corpus callosum: Pushed down/flattened profile and appears thick in sagittal profile	Corpus callosum pushed up and appears thinned out in sagittal plane
AC is in the same plane or lower than PC	PC is either same or slightly lower than AC	AC is either in the same level or slightly higher than PC
	The outer surface of CC appears buckled down	Waviness of the inner surface of CC and is directed upward
Calloso-septal angle	Maintained to increased angle but have an elongated profile	Ballooned out and reduced angle
Tentorium and venous sinus	Tentorium stretched and pushed down	Tentorium stretched and pushed down
Plain and postcontrast figure	SSS appears more prominent	SSS appears normal, transverse sinus normal
Arachnoid granulation	Mid-third transverse sinus at bony prominence narrowed	Straight sinus is stretched
Line of torque	Straight sinus is stretched	Normal arachnoid granulation
	Arachnoid granulations are very prominent in the cisterns	
Sella MCF	Empty sella	Empty sella
Parenchymal changes	Subcortical and deep white-matter hyperintensities	Periventricular hyperintensities and periventricular ooze (bulk water) with deep white-matter hyperintensities
		Prominent VR spaces
Infratentorium: PCF and brainstem structures, cerebellum, brainstem, and spinal cord		
Brainstem	Mamillopontine profile	Mamillopontine profile
Cervicomedullary angle and pontomesencephalic angle	Appears buckled downward	Appears opened up due to prominent cisterns
	Appears to have acute angulation	Appears to have an obtuse angulation

Contd...

Table 1: Contd...

Summary of the morphological changes in the brain in IIH and NPH		
Controls	**IIH**	**NPH**
Cerebellum PCF	Cerebellum elongated appearance in sagittal orientation (tonsillar herniation is known). Sagittal plane cerebellum appears rotated counterclockwise as cerebellum is pushed down	Cerebellum appears buckled upward by cisterns around (cerebellar foliae and fissure appear prominent) Sagittal plane: Cerebellum appears rotated clockwise as cerebellum is lifted up
Prepontine cistern and IV ventricle	Narrow prepontine cisterns based on the degree of inferior shift, fourth ventricle appears small in dimensions	Prepontine cisterns prominent Cisterns, for example, mega cistern magna Reservoir Fourth ventricle appears en larged with prominent flow void
Craniospinal axis and spinal cord	IIH; the spinal nerve sheath prominent (ectasia in few cases) and a normal central canal	NPH; the spinal nerve sheath appears normal with mild prominence of central canal
Other zones of drainage/buffering areas (such as perineural sheath, perivascular spaces [VR spaces], cisterns, and subarachnoid spaces)	Prominent Optic nerve sheath prominent with tortuous course optic nerve SAS around olfactory nerve prominent Acoustic nerve sheath normal Spinal nerve root sheath prominent (meningoceles are known in literature) Meckels cave prominent	Prominent Optic nerve sheath prominent but course of optic nerve not tortuous SAS around olfactory nerve prominent Acoustic nerve sheath prominent Spinal nerve root sheath normal Meckels cave normal

CSF – Cerebrospinal fluid; TBV – Total brain volume; ICV – Intracerebral volume; FLAIR – Fluid-attenuated inversion recovery sequence; ACF – Anterior cranial fossa; MCF – Middle cranial fossa; VR – Virchow–Robin; PCF – Posterior cranial fossa; IIH – Idiopathic intracranial hypertension; NPH – Normal pressure hydrocephalus; SAS – Subarachnoid space; AC – Anterior commissure; PC – Posterior commissure; CC – Corpus callosum; TL – Temporal lobe

LP opening pressure, whereas in NPH, increased velocity in the IV ventricle is noted on imaging.

Reviewing all the imaging findings, routine MRI findings in IIH are already discussed above and invasive DSA shows a pressure gradient in sigmoid sinus stenosis (SSS) and TS in IIH.[3] Invasive Transmantle study shows decreased absorption and increased pressure at SAS in NPH and IIH.[13,14] Volume distribution of GM, WM, and CSF was found to be similar to controls in both IIH and NPH in our study. Phase MRI four-dimensional (4D) studies show increased flow velocity in NPH and IIH.[15,16] Cine displacement encoding with stimulated echo (DENSE) images in healthy controls have shown brain motion in synchronization with cardiac pulsation in the following order: optic chiasma > brainstem > occipital, cerebellum and frontal and parietal lobe, The time to peak of the normal wave of pulsatile movement of the brain throughout the cardiac cycle was from the brain stem to cerebellum to optic chiasma to the peripheral brain lobes (occipital to parietal to frontal)[17] in controls. In IIH on DENSE imaging there was decrease in pulsatility with decreased superoinferior pontine displacement.[18] DENSE imaging pattern in NPH needs to be explored. In NPH and IIH, glylymphatic MRI 4D has shown decreased clearance of intrathecal gadolinium from SAS via the parenchyma into the venous system with an increased gadolinium leakage into parenchyma from both the cortical and transependymal surfaces.[8,12] Similar phenomenon with metabolic waste in CSF leading to amyloid and tau in CSF and deposition has been described in other studies.[19,20] A study using elastography five-dimensional (5D) imaging has shown decreased elasticity and increased stiffness of brain parenchyma in IIH, which is very similar to stiff brain found on histopathology.[14,21] Elastography study in NPH has shown that stiffness was increased in cerebrum and parietal, occipital, and temporal lobes, and they suggest that increased ventricular dilatation causes interstitial and intracellular fluid to be squeezed out of parenchymal pores, leading to increased stiffness and loss of compliance.[22] An elastography study in porcine model has shown that, when a normal brain tissue is subject to stress and strain by mechanical pressure due to raised ICP, it migrates from a linear fashion to nonlinear fashion and the stiffness increases, but brain function can still occur in this zone, which can explain the chronic indolent course in IIH and NPH.[23] Artery is one of the most important core drivers of ICP. For phase imaging on MRI, the values for velocity encoding are approximately an average of 50 cm/s (60–150 cm/s) for cerebral artery, 35 cm/s (10–60 cm/s) for cerebral veins, and 10 cm/s (2–20 cm/s) for CSF in the aqueduct and spinal SAS.[24] In conditions of decompensation leading to raised ICP like in CVT and IIH

due to venous outflow block, the venous pressure can go up to arterial velocities[25] and in acute hydrocephalus and NPH, CSF pressure can be equivocal venous velocities. This phenomenon may explain the cause of decompensation and congestion in these cases.

Both IIH and NPH are physiological changes which occur over longer time and hence structural MRI may not be sufficient to make a diagnosis. Both have an abnormal baseline with periods of relapse and remission based on the pressure gradient difference in the arterial venous and CSF compartments. As a part of abnormal baseline, there may be decreased elasticity causing remolding of shape of brain contents with a normal ICP during remission followed by sudden deterioration and acute raise in ICP during periods of relapse. Detailed physiological studies such as flow studies, Transcranial Doppler (TCD), and elastography are limited in these conditions comparing relapse and remission phases.

We have noted the shape changes in brain morphology, SAS, and WM bundles as an indirect marker for the way the brain may have been squeezed, keeping in mind the location and compartments of brain in vault and also its unique shape.

Based on the clinical and imaging findings and review of findings in other studies, we have built a hypothetical model for IIH and NPH and they appear to be different faces of the same coin and we have enlisted below why they appear same and the location of inverted mirror images [Table 2].

Why termed same coin

Papillodema is a feature of IIH and not NPH, reflecting its malignant clinical course.[26,27] Biophysics wise, mechanical strain is the result with break point being increased venous pressure in IIH and increased CSF velocity in NPH. A model based on MK hypothesis and the four compartments in healthy controls is represented in Figure 1b. Symptomatic relief is obtained when this vicious cycle is broken by interventions such as stent shunt.[2] Since brain CSF and veins are passive outflow system with no means to pump out independently other than by arterial pulsation and passive displacement, currently, only the above interventions work in both.

Why termed different sides of the same coin based on the postulated model

Direction of the brain shift due to increased venous pressure/CSF velocity is different, and etiology for the starting point of induction of the loop of IIH and NPH is different. The subarachnoid space in the parietal convexity is prominent in IIH[28] and effaced in NPH [Figure 3b]. In both these entities, however, since skull vault is fixed, the brain is shifted either inferiorly or superiorly, the line which experiences the maximum torque is in sagittal

Table 2: Summary of why idiopathic intracranial hypertension and normal pressure hydrocephalus are termed the same coin and different sides of the same coin

Same coin	**IIH and NPH**	**Variation**
Idiopathic	No structural lesion but functional-level changes	Core drivers are different
LP drainage	Improvement in both	Additional venous stenting in IIH or shunting of CSF in NPH
Imaging	Empty sella and optic nerve sheath dilatation in both	Papillodema absent in NPH but present in IIH
Course clinically	Chronic progressive disorders with relapse and remission in both	Causative factors are different
Clinical features	Vague and varied with a wide spectrum of causes and presentation in both	
Different sides of the same coin	**IIH**	**NPH**
Model and core drivers	Increase venous pressure	Increased CSF velocity
Postulated model of brain shift which is in equilibrium with no pressure gradient in normal		
Sagittal	Anteroinferior direction (exaggeration of normal tilt)	Posterosuperior direction shift
Coronal	Features of centrifugal gradient and SAS-effaced	Features of centripetal gradient and SAS-enlarged
	Herniation features	reverse herniation features
Axial	Centrifugal pressure gradient	Centripetal pressure gradient
Clinical presentation	Cranial nerve involvement headache	PD like, gait, memory, etc.
Imaging	Juxta and deep WM changes	Periventricular and deep WM changes
Complication	Intracranial hypotension	Acute hydrocephalus

CSF – Cerebrospinal fluid; IIH – Idiopathic intracranial hypertension; NPH – Normal pressure hydrocephalus; LP – Lumbar puncture; SAS – Subarachnoid space; WM – White matter

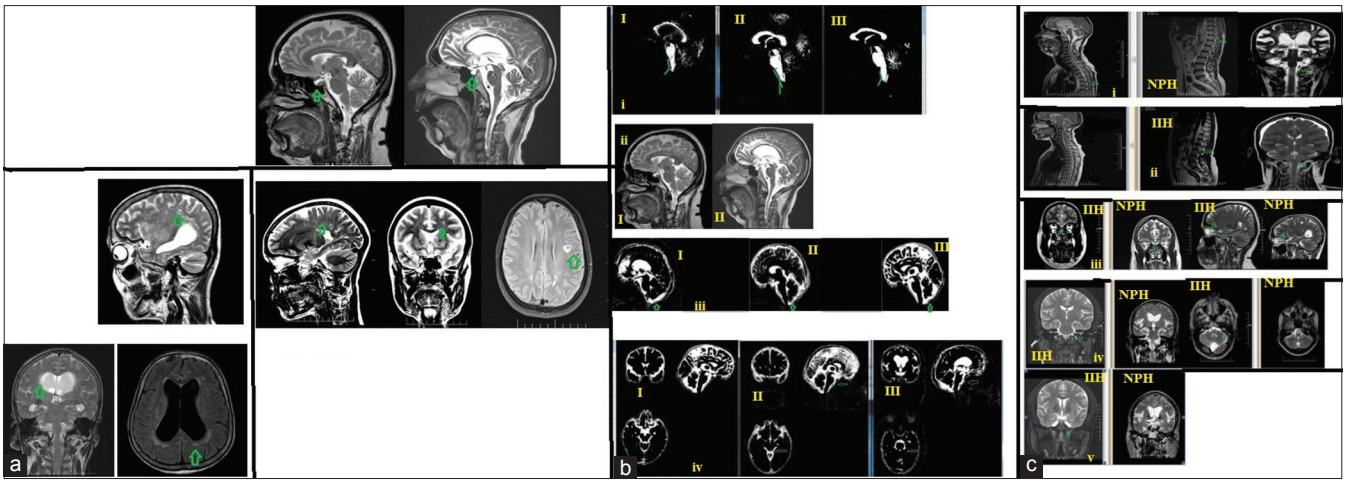

Figure 4: (a) (i-iii) Sella and parenchymal changes: (i) Empty sella in (I) idiopathic intracranial hypertension and (II) normal pressure hydrocephalus. (i and iii) Periventricular white matter hyperintensities at corona radiata, lateral ventricle, and sagittal sections; (ii) parenchymal changes at idiopathic intracranial hypertension. Idiopathic intracranial hypertension has more lateral and subcortical hyperintensity; (iii) parenchymal changes in normal pressure hydrocephalus. Normal pressure hydrocephalus has more periventricular white matter hyperintensity. These changes may act as an indirect marker of transmantle pressure resulting in the change of glylymphatic flow and related white-matter changes. (b) (i-iv) Infratentorial changes on magnetic resonance imaging: (i) Brainstem in (I) normal pressure hydrocephalus, (II) idiopathic intracranial hypertension, (III) normal on white-matter segmented data: (I) Normal pressure hydrocephalus cervicomedullary angle and pontomesencephalic angle have an obtuse configuration and normal-to-increased mamillopontine distance, (II) idiopathic intracranial hypertension: cervicomedullary angle: the pontomesencephalic angle is lost and in line with normal-to-decreased mamillopontine distance. (III) Normal configuration of cervicomedullary angle and maintained mamillopontine distance. (ii) Magnetic resonance imaging mid-sagittal view in idiopathic intracranial hypertension and normal pressure hydrocephalus brainstem configuration. (iii) In this ventriculogram-like image the cerebellar configuration and cisterns around it were assessed in. (I) Normal pressure hydrocephalus, (II) idiopathic intracranial hypertension, (III) controls. (I) Normal pressure hydrocephalus cerebellum appears buckled upward by cisterns around with clockwise upward rotation of cerebellum, (II) idiopathic intracranial hypertension cerebellum elongated appearance in sag orientation with counterclockwise rotation of cerebellum, (III) normal position of cerebellum. (iv) Ventriculogram-like picture: prepontine cistern and IV ventricle. (I) normal, (II) idiopathic intracranial hypertension of prepontine cistern narrow with small IV ventricle, (III) normal pressure hydrocephalus of prepontine cistern and IV ventricle appears prominent with flow void. (c) (i and ii) Other routes of cerebrospinal fluid drainage such as spinal nerve sheath along the craniospinal axis. (i) Normal pressure hydrocephalus: normal dimensions of SAS along the spinal nerve sheath noted associated with mild prominence of central canal as seen in sagittal and coronal view of cervical and lumbar spine (ii) idiopathic intracranial hypertension: the prominent spinal nerve sheath (ectasia in few cases) with normal dimensions of the central canal in sag and coronal view of cervical and lumbar spine. (c)(iii-v)Unconventional zones of drainage along the spinal and cranial nerve roots to extracranial lymph nodes in idiopathic intracranial hypertension and normal pressure hydrocephalus, (iii-v) (iii) periolfactory nerve sheath in idiopathic intracranial hypertension and normal pressure hydrocephalus and perioptic nerve sheath in idiopathic intracranial hypertension and normal pressure hydrocephalus, (iv) Internal auditory canal nerve sheath of 7–8 nerves in idiopathic intracranial hypertension and normal pressure hydrocephalus (coronal and axial sections) and (v) Meckels cave of V nerve in idiopathic intracranial hypertension and normal pressure hydrocephalus

orientation at the prefrontal > occipital region termed as "the line or axis of maximum torque at the level of lateral ventricles where diameter was maximum in axial plane and sagittal. The other line of torque was in midline along the CC and brainstem, with the fulcrum of both these points lying on the third ventricle as noted in coronal and axial planes. These lines may explain the decreased pulsatility in this plane as noted in other studies.[18]

In controls on imaging (coronal plane) the lateral ventricles are larger than the SAS with no evidence of herniation or midline shift [Figure 1b]. In IIH, centrifugal forces act [Figure 5a] with features of herniation and in NPH centripetal forces act with features of reverse herniation [Figure 5b].

In a state of equilibrium on axial imaging keeping the model of brain with CSF flow in VR and glylymphatics, there is a state of equivocal centrifugal and centripetal forces [Figure 1b]. In IIH, centrifugal forces work on the brain parenchyma due to increased venous back pressure from superficial cortical veins back to venules in the brain parenchyma resulting in pressure at the cortical margin, which is bone–brain interface and also on the lateral ventricles which passively collapse [Figure 5a]. In case of NPH, centripetal forces work on the brain parenchyma due to increased CSF back pressure from SAS back to lateral ventricles, resulting in increased velocity of CSF through the craniospinal axis and pressure dissipation onto brain parenchyma from ventricular and cortical surfaces of brain [Figure 5b].

The normal physiology of brain parenchyma is not visible in a structural MRI. However, there is a dynamic balance between various compartments, which makes the brain have a particular profile on routine MRI as shown in the postulated model of a normal control. The physiology of brain across various compartments has been drawn to understand this fine balance [Figure 5]. In case of IIH [Figure 5a] and NPH [Figure 5b], a similar model has been built to understand the physiology.

The MK 2.0 focuses on venous pressure as a core driver[1] causing impaired glymphatic drainage in

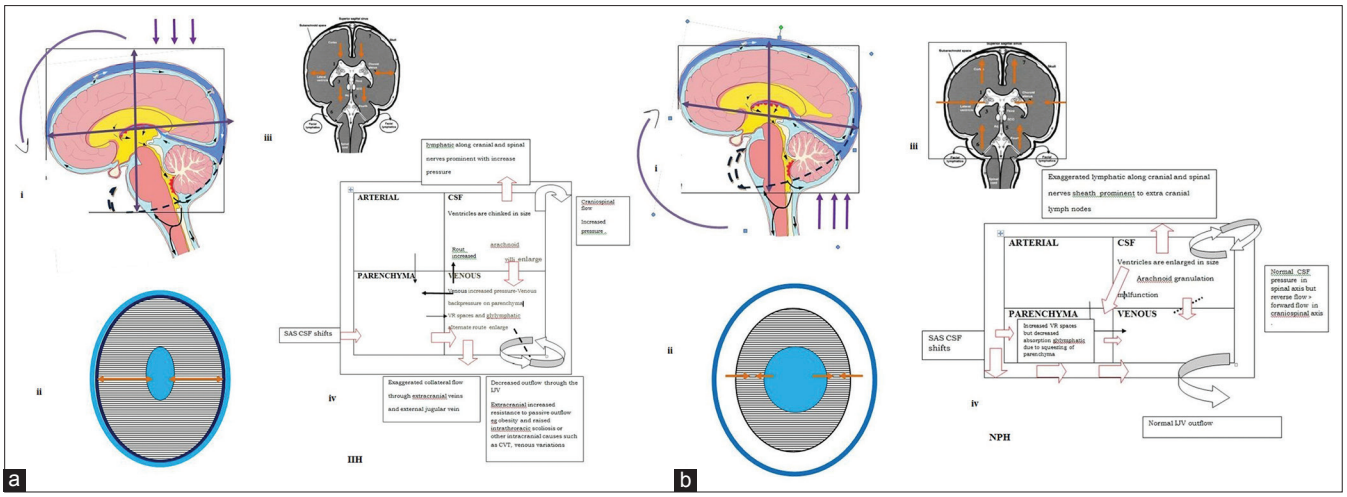

Figure 5: (a) (i-iv) Postulated model in a case of idiopathic intracranial hypertension as supported by imaging findings. In a case of idiopathic intracranial hypertension, the possible mechanism is increased venous pressure in the venous sinus rather than venous velocity or volumes with differing distribution of venous pressure gradient based on anatomy. The midline structures such as corpus callosum, cerebrospinal fluid, and brainstem have more freedom of translation than the laterally placed structures such as temporal and frontal poles. Sigmoid sinus stenosis secondary to increased pressure, especially at the high convexity veins such as Superior saggital sinus , where the diameter is maximum, making the floating brain experience an exaggeration of the normal torsion in the anteroinferior direction with fulcrum in the midline. The brain parenchyma acts as a buffering zone to some extent, and the increased back pressure causes venous congestion in brain parenchyma. Brain shifts due to increased cerebral venous pressure causing secondary subarachnoid space cerebrospinal fluid redistribution within the various compartments as mentioned above. Increased stiffness of brain parenchyma may be due to both congestion and the shift. (i) Sagittal: representative image for the hypothesis in this case is that there is an exaggeration of the normal anteroinferior torsion of brain parenchyma in the skull in the sagittal plane, (ii) centrifugal pressure gradient transmitted from brain parenchyma to the surrounding due to venous congestion and venous back pressure as shown in axial images, (iii) coronal image: anterior and inferior (downward) torsion. Due to the net torsion in all planes brain is maximally squeezed in the prefrontal-occipital lobes plane along with venous congestion. Due to this brain shift in anterio inferior direction , there is paradoxical prominence of the high frontal and high parietal subarachnoid spaces, and due to impaired CSF absorption and increased back pressure transmitted to cerebrospinal fluid, structures in anterior cranial fossa, middle cranial fossa which act as secondary extracranial CSF draining sites such as sella and neural forminal sheath) are prominent. Posterior fossa structures also experience torque in the inferior direction. The transmantle pressure gradient is centrifugalin nature due to venous congestion and back pressure changes resulting in pressure dissipation both on the ventricular surface and the cortical margins. The pressure gradient is maximum on the subcortical location as the cortex gets pressed against the skull bone in the axial section at the level of ventricles. The brain is also remolded to have a brachy appearance. The push on the posterior fossa in the mid coronal image is represented with herniation inferiorly and effacement of subarachnoid space in the prefrontal and occipital regions and chinked appearance of lateral ventricle. Downward minor shifts are known with prominent subarachnoid space and cranial nerve sheath. Downward displacement of parenchyma through Kernohan's notch/transformaminal herniation can happen when it reaches a state of decompensation. (iv) Monroe–Kellie model and venous and cerebrospinal fluid circulation in idiopathic intracranial hypertension. The shape of the boxes has been maintained the same (as volumes are maintained the same ,unlike in other models of raised intracranial pressure where volumes of individual compartment change. (b) (i-iv) Postulated model in a case of normal pressure hydrocephalus supported by imaging findings. Sagittal, coronal, and axial: In a case of idiopathic normal pressure hydrocephalus, the possible mechanism is decreased cerebrospinal fluid absorption in the craniospinal axis leading to an increased cerebrospinal fluid velocity. The midline structures such as corpus callosum, cerebrospinal fluid, and brainstem have more freedom of translation than that of the laterally placed structures such as temporal and frontal poles. Increased velocity of cerebrospinal fluid and the retrograde flow cause a displacement of the floating brain, and it experiences a torsion in the posterior and superior directions. The brain parenchyma acts as a buffering zone for this, and the increased velocity of cerebrospinal fluid is redistributed in the brain tissue in differing gradients resulting in increased stiffness of brain parenchyma and secondary subarachnoid space effacement. (i) Sagittal: The representative image for the hypothesis in this case is that there is a posterosuperior torsion of brain parenchyma in the skull in the sagittal plane, (ii) Axial: centripetal pressure gradient transmitted from subarachnoid space and intraventricular cerebrospinal fluid to the brain parenchyma as shown in axial images (iii) coronal image torsion axis posterior and superior [upward]). Due to the net torsion in all planes brain is maximally squeezed in the prefrontal-occipital lobes plane. Due to the brain shift superiorly, the high parietal subarachnoid space is effaced. The cerebrospinal fluid in anterior cranial fossa and middle cranial fossa (sella and neural forminal sheath) is prominent due to passive displacement. Posterior fossa structures also experience torque in superior direction. The transmantle pressure gradient is centripetal in nature secondary to cerebrospinal fluid back pressure changes resulting in pressure dissipation on the subependymal surface and cortical surface. The periventricular space which contains white matter bundles has more elasticity than cortical gray matter. The brain is molded to have a long and narrow dolicho like appearance. The push on the posterior fossa in the midcoronal image is represented with reverse herniation superiorly and effacement of subarachnoid space in the prefrontal-occipital plane with prominent and dilated lateral ventricles. The subarachnoid space are prominent along cranial nerve sheath due to stagnation of CSF. (iv) Monroe–Kellie model and venous and cerebrospinal fluid circulation in normal pressure hydrocephalus. The shape of the boxes has been maintained the same unlike in other models of raised intracranial pressure where volumes of individual compartment change, as in this condition, volume is the same

IIH.[12,14] In postcontrast study in IIH, all veins were prominent except the mid third of TS [Figure 3d], and a dynamic increase or decrease in arterial flow and collateral to external jugular vein and stenoses at TS was noted,[8,29,30] suggesting a brain shift as the possible cause and that venous pressure is the core driver and stenosis is an epiphenomenon of IIH and not the cause. The paradoxical prominence of parietal SAS in raised intracranial pressurecan be explained by brain shift suggested in MK 3.0.

NPH, the trigger point, is the decreased SAS absorption leading to changes in craniospinal axis as noted in a study where CSF outflow resistance was >18 cmH_2O/ml/min (normal <8 cmH_2O/ml/min)[13] and

shunt is a treatment. Disproportionately enlarged subarachnoid space hydrocephalus (DESH) and effaced parietal sulci[2] can be explained by MK 3.0.

For the ease of modeling the pathophysiology though we have shown brain as an ovoid and skull as a rectangular box around it, it is more complex due to the various fossae and compartments formed by dural attachment, bone and venous sinuses. The central brain has more freedom of shift than the lateral brain as noted on elastography and DENSE studies.[16,18] In IIH, we hypothesise that there is centrifugal mechanical stress and as a result of this shear strain, on cortex and overlying dura and veins there may be neuronal cortical depression and pain induction causing headache.[31] The inferior torque induces vomiting and diplopia.[1] Pressure transmission from perineural SAS of cranial nerve may cause cranial neuralgia. Chronic mechanical stretching and increased pressure in line of torque lying along the prefrontal and occipital pole may result in occipital migraine and CSF rhinoorhoea due to bony erosion of thin lamina papyracea.[1] Spontaneous intracranial hypotension may be complication of long standing intracranial hypertension with the perineural sheath along the spinal nerve acting as a sudden give away point to raised pressure in the SAS.[1]

In NPH in line with our model, there may be decreased periventricular perfusion due to mechanical stress leading to stretching of corona radiate fibres and hence the features of gait abnormality. Stretching of the cortico spinal tracts may cause lower body PD and pyramidal signs. High convexity parietal lobe compression may cause acalculia and paracentral lobule compression may cause urinary incontinence.[2] The combined pressure on the cortical surface and the fornices may explain the cause cognitive changes with AD and FTD like presentation. A study has shown decreased CBF in the basal medial frontal cortex and deep gray matter in NPH which correlates with severity of clinical symptoms. DTI measures of neuronal integrity have shown changes in corona radiata, CC, frontal lobe The increased T2 signal and decreased elasticity has been attributed to brain softening and leading to small vessel disease changes[22] which may further worsen the glymphatic drainage in NPH.

The juxta/subcortical and deep WM are more elastic. Centrifugal gradient in IIH and centripetal gradient in NPH make hyperintensity in subcortical location in IIH and periventricular (PV) location in NPH [Figure 4a], with increased apparent diffusion coefficient values noted.[14,32] Venous watershed zone is between PV/deep WM with cortical/subcortical WM, and this area is hence prone in both IIH and NPH. Differential tissue density mantles and mechanical stress cause a unique pattern of cortical/subcortical changes in IIH and ependymal PVWM zone in NPH. The computational model has shown similar points of mechanical stress and blood oxygenation level-dependent perfusion venous lag in superficial and deep venous systems, confirming our centrifugal and centripetal pressure gradients in IIH and NPH, respectively.[7] T2 images of frontal WM and GM at cortex and deep WM showed decreased pixel values in IIH and increased values in NPH, likely secondary change in the elastic property of tissue. T2 hypointensity is due to nonheme iron as in venous congestion,[34] and a similar phenomenon is seen in IIH.

As already highlighted in the beginning of the discussion, review of basic and advanced imaging demonstrate the phenomenon of decreased pulsatility.[18] high cortical venous pressure and decreased glylymphatic drainage[12] in IIH. and increased velocity and decreased forward flow[3] and decreased clearance of gadolinium[8] in NPH respectively. The same has been shown in our postulated model. A similar phenomenon may be happening with metabolic waste in CSF, leading to amyloid and tau deposition.[19] along the PV surface[35] and parietal areas secondary to stress and strain.[36]

The mechanism of cognitive changes in IIH and dementia in NPH would be interesting as this would be a reversible cause of dementia. Positron emission tomography studies in NPH have shown global decrease in CBF,[37] and decreased glylymphatic drainage may be the prime cause for neurodegeneration.[12,38] Multidomain cognitive impairment in IIH has been noted.[39] T2 prolongation in Alzheimer's disease which is associated with NPH[40] may be due to increased amyloid deposition in response to strain.

There is loss of buffering causing small vessel ischemic changes on imaging in chronic arterial hypertensive encephalopathy.[41] Similar changes may be noted in IIH, which is a chronic venous hypertensive encephalopathy.

Few lessons were learned from complication in IIH and NPH in relation to MK 3.0 hypothesis.

Intracranial hypotension has a cluster of imaging features contrary to that of IIH.[42,43] Various angles such as pontomesencephalic angle, mamillopontine distance, and lateral ventricular angle are altered in hypotension and IIH.[43] Sudden decrease in venous pressure (core driver) may exaggerate inferior shift in hypotension. Phase-contrast MRI in IIH has shown decreased CSF flow in rate in aqueduct in IIH and lumboperitoneal shunt may worsen this flow.[15] Sella volumes are reversible in IIH and hypotension though pituitary remains functional in response to stress. A similar phenomenon is noted in brain parenchyma.

NPH is known to have CSF tau and beta and synucleinopathy/taupathy similar to other neurodegenerative disorders.[44-46] Altered CSF dynamics due to mechanical stress may result in metabolic waste deposit in these disorders.

Conclusion

Overall, at the end of this study, we are tempted to replace "idiopathic" term with chronic venous hypertensive encephalopathy in IIH and chronic hydrocephalic encephalopathy in NPH. CINE DENSE imaging which

maps brain movement may help diagnose faulty venous and CSF hydraulics.

Financial support and sponsorship

Nil.

Conflicts of interest

There are no conflicts of interest.

References

1. Suzuki H, Takanashi J, Kobayashi K, Nagasawa K, Tashima K, Kohno Y. MR imaging of idiopathic intracranial hypertension. AJNR Am J Neuroradiol 2001;22:196-9.
2. Damasceno BP. Neuroimaging in normal pressure hydrocephalus. Dement Neuropsychol 2015;9:350-5.
3. Goodwin CR, Elder BD, Ward A, Orkoulas-Razis D, Kosztowski TA, Hoffberger J, *et al.* Risk factors for failed transverse sinus stenting in pseudotumor cerebri patients. Clin Neurol Neurosurg 2014;127:75-8.
4. Gölz L, Ruppert FH, Meier U, Lemcke J. Outcome of modern shunt therapy in patients with idiopathic normal pressure hydrocephalus 6 years postoperatively. J Neurosurg 2014;121:771-5.
5. Markey KA, Mollan SP, Jensen RH, Sinclair AJ. Understanding idiopathic intracranial hypertension: Mechanisms, management, and future directions. Lancet Neurol 2016;15:78-91.
6. Wilson MH. Monro-Kellie 2.0: The dynamic vascular and venous pathophysiological components of intracranial pressure. J Cereb Blood Flow Metab 2016;36:1338-50.
7. Kim H, Min BK, Park DH, Hawi S, Kim BJ, Czosnyka Z, *et al.* Porohyperelastic anatomical models for hydrocephalus and idiopathic intracranial hypertension. J Neurosurg 2015;122:1330-40.
8. Ringstad G, Vatnehol SA, Eide PK. Glymphatic MRI in idiopathic normal pressure hydrocephalus. Brain 2017;140:2691-705.
9. Cherian I, Beltran M, Kasper EM, Bhattarai B, Munokami S, Grasso G, *et al.* Exploring the Virchow-Robin spaces function: A unified theory of brain diseases. Surg Neurol Int 2016;7:S711-4.
10. Engelhardt B, Carare RO, Bechmann I, Flügel A, Laman JD, Weller RO, *et al.* Vascular, glial, and lymphatic immune gateways of the central nervous system. Acta Neuropathol 2016;132:317-38.
11. Orešković D, Klarica M. A new look at cerebrospinal fluid movement. Fluids Barriers CNS 2014;11:16.
12. Bezerra ML, Ferreira AC, de Oliveira-Souza R. Pseudotumor cerebri and glymphatic dysfunction. Front Neurol 2017;8:734.
13. Ramesh VG, Narasimhan V, Balasubramanian C. Cerebrospinal fluid dynamics study in communicating hydrocephalus. Asian J Neurosurg 2017;12:153-8.
14. Gideon P, Sørensen PS, Thomsen C, Ståhlberg F, Gjerris F, Henriksen O, *et al.* Increased brain water self-diffusion in patients with idiopathic intracranial hypertension. AJNR Am J Neuroradiol 1995;16:381-7.
15. Akay R, Kamisli O, Kahraman A, Oner S, Tecellioglu M. Evaluation of aqueductal CSF flow dynamics with phase contrast cine MR imaging in idiopathic intracranial hypertension patients: Preliminary results. Eur Rev Med Pharmacol Sci 2015;19:3475-9.
16. Tawfik AM, Elsorogy L, Abdelghaffar R, Naby AA, Elmenshawi I. Phase-contrast MRI CSF flow measurements for the diagnosis of normal-pressure hydrocephalus: Observer agreement of velocity versus volume parameters. AJR Am J Roentgenol 2017;208:838-43.
17. Zhong X, Meyer CH, Schlesinger DJ, Sheehan JP, Epstein FH, Larner JM, *et al.* Tracking brain motion during the cardiac cycle using spiral cine-DENSE MRI. Med Phys 2009;36:3413-9.
18. Saindane AM, Qiu D, Oshinski JN, Newman NJ, Biousse V, Bruce BB, *et al.* Noninvasive assessment of intracranial pressure status in idiopathic intracranial hypertension using displacement encoding with stimulated echoes (DENSE) MRI: A prospective patient study with contemporaneous CSF pressure correlation. AJNR Am J Neuroradiol 2018;39:311-6.
19. Graff-Radford NR. Alzheimer CSF biomarkers may be misleading in normal-pressure hydrocephalus. Neurology 2014;83:1573-5.
20. Radford RA, Morsch M, Rayner SL, Cole NJ, Pountney DL, Chung RS, *et al.* The established and emerging roles of astrocytes and microglia in amyotrophic lateral sclerosis and frontotemporal dementia. Front Cell Neurosci 2015;9:414.
21. Kolipaka A, Wassenaar PA, Cha S, Marashdeh WM, Mo X, Kalra P, *et al.* Magnetic resonance elastography to estimate brain stiffness: Measurement reproducibility and its estimate in pseudotumor cerebri patients. Clin Imaging 2018;51:114-22.
22. Fattahi N, Arani A, Perry A, Meyer F, Manduca A, Glaser K, *et al.* MR elastography demonstrates increased brain stiffness in normal pressure hydrocephalus. AJNR Am J Neuroradiol 2016;37:462-7.
23. Arani A, Min HK, Fattahi N, Wetjen NM, Trzasko JD, Manduca A, *et al.* Acute pressure changes in the brain are correlated with MR elastography stiffness measurements: Initial feasibility in an *in vivo* large animal model. Magn Reson Med 2018;79:1043-51.
24. Balédent O. Imaging of the Cerebrospinal Fluid Circulation Adult Hydrocephalus. UK: Cambridge University Press; 2014. p. 121-38.
25. Valdueza JM, Hoffmann O, Weih M, Mehraein S, Einhäupl KM. Monitoring of venous hemodynamics in patients with cerebral venous thrombosis by transcranial Doppler ultrasound. Arch Neurol 1999;56:229-34.
26. Gourdeau A, Miller NR. Neuro Ophthalmological Signs of Hydrocephalus, Neurobiology of Cerebrospinal Fluid 2. New York: Plenum Press; 1983.
27. Ertl M, Aigner R, Krost M, Karnasová Z, Müller K, Naumann M, *et al.* Measuring changes in the optic nerve sheath diameter in patients with idiopathic normal-pressure hydrocephalus: A useful diagnostic supplement to spinal tap tests. Eur J Neurol 2017;24:461-7.
28. Alperin N, Ranganathan S, Bagci AM, Adams DJ, Ertl-Wagner B, Saraf-Lavi E, *et al.* MRI evidence of impaired CSF homeostasis in obesity-associated idiopathic intracranial hypertension. AJNR Am J Neuroradiol 2013;34:29-34.
29. Bateman GA. Vascular hydraulics associated with idiopathic and secondary intracranial hypertension. AJNR Am J Neuroradiol 2002;23:1180-6.
30. Bateman GA. Arterial inflow and venous outflow in idiopathic intracranial hypertension associated with venous outflow stenoses. J Clin Neurosci 2008;15:402-8.
31. Ray BS, Wolff HG. Experimental studies on headache pain-sensitive structures of the head and their significance in headache. Arch Surg 1940;41:813-56.
32. Walker RW. Idiopathic intracranial hypertension: Any light on the mechanism of the raised pressure? J Neurol Neurosurg Psychiatry 2001;71:1-5.
33. Satow T, Aso T, Nishida S, Komuro T, Ueno T, Oishi N, *et al.* Alteration of venous drainage route in idiopathic normal pressure hydrocephalus and normal aging. Front Aging Neurosci 2017;9:387.
34. Kamble JH, Parameswaran K. "Venous congestion" as a cause of subcortical white matter T2 hypointensity on magnetic resonance images. Ann Indian Acad Neurol 2016;19:411-3.
35. Hakim S, Venegas JG, Burton JD. The physics of the cranial

cavity, hydrocephalus and normal pressure hydrocephalus: Mechanical interpretation and mathematical model. Surg Neurol 1976;5:187-210.

36. Bateman GA. The pathophysiology of idiopathic normal pressure hydrocephalus: Cerebral ischemia or altered venous hemodynamics? AJNR Am J Neuroradiol 2008;29:198-203.
37. Brooks DJ, Beaney RP, Leenders KL, Marshall J, Thomas DJ, Jones T, *et al.* Regional cerebral oxygen utilization, blood flow, and blood volume in benign intracranial hypertension studied by positron emission tomography. Neurology 1985;35:1030-4.
38. Jagust WJ, Friedland RP, Budinger TF. Positron emission tomography with [18F]fluorodeoxyglucose differentiates normal pressure hydrocephalus from Alzheimer-type dementia. J Neurol Neurosurg Psychiatry 1985;48:1091-6.
39. Zur D, Naftaliev E, Kesler A. Evidence of multidomain mild cognitive impairment in idiopathic intracranial hypertension. J Neuroophthalmol 2015;35:26-30.
40. Knight MJ, McCann B, Tsivos D, Dillon S, Coulthard E, Kauppinen RA, *et al.* Quantitative T2 mapping of white matter: Applications for ageing and cognitive decline. Phys Med Biol 2016;61:5587-605.
41. Schwartz RB, Jones KM, Kalina P, Bajakian RL, Mantello MT, Garada B, *et al.* Hypertensive encephalopathy: Findings on CT, MR imaging, and SPECT imaging in 14 cases. AJR Am J Roentgenol 1992;159:379-83.
42. Kranz PG, Tanpitukpongse TP, Choudhury KR, Amrhein TJ, Gray L. Imaging signs in spontaneous intracranial hypotension: Prevalence and relationship to CSF pressure. AJNR Am J Neuroradiol 2016;37:1374-8.
43. Shah LM, McLean LA, Heilbrun ME, Salzman KL. Intracranial hypotension: Improved MRI detection with diagnostic intracranial angles. AJR Am J Roentgenol 2013;200:400-7.
44. Narita W, Nishio Y, Baba T, Iizuka O, Ishihara T, Matsuda M, *et al.* High-convexity tightness predicts the shunt response in idiopathic normal pressure hydrocephalus. AJNR Am J Neuroradiol 2016;37:1831-7.
45. Hong YJ, Kim MJ, Jeong E, Kim JE, Hwang J, Lee JI, *et al.* Preoperative biomarkers in patients with idiopathic normal pressure hydrocephalus showing a favorable shunt surgery outcome. J Neurol Sci 2018;387:21-6.
46. Starr BW, Hagen MC, Espay AJ. Hydrocephalic parkinsonism: Lessons from normal pressure hydrocephalus mimics. J Clin Mov Disord 2014;1:2.